JOURNAL OF MATERIALS SCIENCE 11 (1976) 1884–1892

Microstructure and brittle behaviour of fine grain calcite (micrite)

J. C. DOUKHAN, J. P. HENRY, J. PAQUET
Laboratoire de Structure et Propriétés de l'Etat Solide (L.A. au CNRS 234), Université des Sciences et Techniques de Lille, 59650 Villeneuve D'Ascq, France

Micrites are natural materials formed by sedimentation in ancient seas. They are generally characterized by a fine grain size and a high compactness. Electron microscopy observations reveal many coincidence boundaries between adjacent grains which allow one to propose a more precise mechanism for the genesis of this material, especially for its high compactness. Moreover, compression tests at various temperatures indicate that micrites are very brittle for $T < 300°$ C. The fracture propagation mechanisms are discussed with the help of the observed microstructure.

1. Introduction

Micrites are very fine-grain limestones ($CaCO_3$) which have been formed in ancient marine environments by lithification of an original ooze. Micrites are generally characterized by a grain size of a few microns and a high compactness reaching 95 to 98% of the theoretical density. The properties of the original ooze are, of course, unknown but one can assume it had a porosity comparable to that of the oozes which are formed at the present time in certain seas (around 50%). The densification process which occurred without heating was, therefore, very efficient. Several explanations have been proposed for this lithification process. All are based on the so-called "recrystallization process" inside the sediment which consists of calcite dissolution in one place followed by its re-precipitation elsewhere, slowly closing the residual pore spaces (see [1] for a review).

We have studied four micrites from the French Jura and the Causses region. It is known from the geological setting that these materials have not been strained or heated [2] and their microstructure is still very close to the original one established after the complete lithification.

The fracture strength, porosity and chemical composition have been measured on the different micrites studied. The results are remarkably homogeneous and the corresponding microstructures are very similar. This indicates that the genesis was probably the same for these four materials.

2. Experimental results

2.1. Porosity

Measurements of volume and mass indicate a proportion of holes of 2 to 4% for all the samples. The volume is deduced from measurements of the edges of finely mechanically polished parallel-epipedic samples. The impurities (mainly aluminosilicate precipitates) do not affect the density deduced because they have almost the same density as calcite. Moreover, samples were dried for two days at 105° C to eliminate water as far as possible.

The open porosity measured with a Hg porosimeter, indicates less than 1% of holes. The difference between these two data is explained by the fact that the Hg porosimeter measures only the open porosity, i.e. the pores which communicate with the external surface. Most of the pores are, therefore, closed. In these tests, we chose unweathered and unfractured samples (Fig. 1).

The open porosity measurements also give a distribution of equivalent pore diameters exhibiting a sharp maximum at 100 to 150 Å. The results, summarized in Table I, show that one kind of micrite (D) is almost wholly dense.

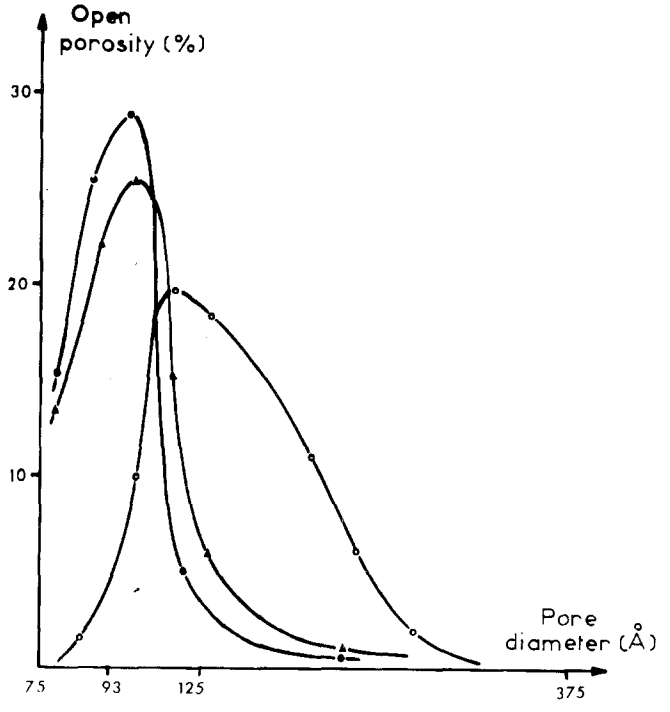

Figure 1 Equivalent pore diameter distribution for the open porosity of the four types of micrites. • micrite A; ○ micrite B; ▲ micrite C. The abscissa is calibrated at regular intervals in a logarithmic scale of pore diameters.

TABLE I Characteristics of the four micrites studied

Property	Micrite A (Fallerans, Doubs)	Micrite B (Etalans, Doubs)	Micrite C (Muret le C., Aveyron)	Micrite D (Vis, Herault)
Statigraphic position	Kimmeridgian	Sequanian	Dogger	Sequanian
Total porosity (%)	2.1 ± 0.4	3.7 ± 0.4	3.3 ± 0.4	2.2 ± 0.4
Open porosity (%)	1	2	1	0
Fracture strength at T_R (daN mm^{-2})	41.5 ± 1.5	40.5 ± 1.5	35 ± 2.5	41.5 ± 1.5
Slope $d\sigma/d\epsilon_1$ (daN mm^{-2})	7800 ± 600	6400 ± 400	6900 ± 300	8200 ± 500
Anisotropy index (%)	16	11	4	12
Fracture strength at $T = 500°$ C	32 ± 1	31 ± 1	29.5 ± 1	30.5 ± 1

2.2. Fracture tests

Uniaxial compression tests were performed on parallelepipedic samples 7 x 7 x 22 mm^3. The faces of the samples were carefully mechanically polished to prevent possible stress concentrations. The defects of parallelism were less than 5 μm. Strain gauges were placed on the faces along the three principal directions to record the deformation of the sample as accurately as possible (either the principal strain ϵ_1 along the compression axis or the volumic strain $\epsilon_V = \epsilon_1 + \epsilon_2 + \epsilon_3$).

2.2.1. Room temperature tests

At room temperature, micrates exhibit a linear elastic behaviour up to the fracture which occurs at $\sigma_F \simeq 40$daN mm^{-2}. The slopes of the stress–strain curves $\sigma(\epsilon_1)$ are approximately equal to the

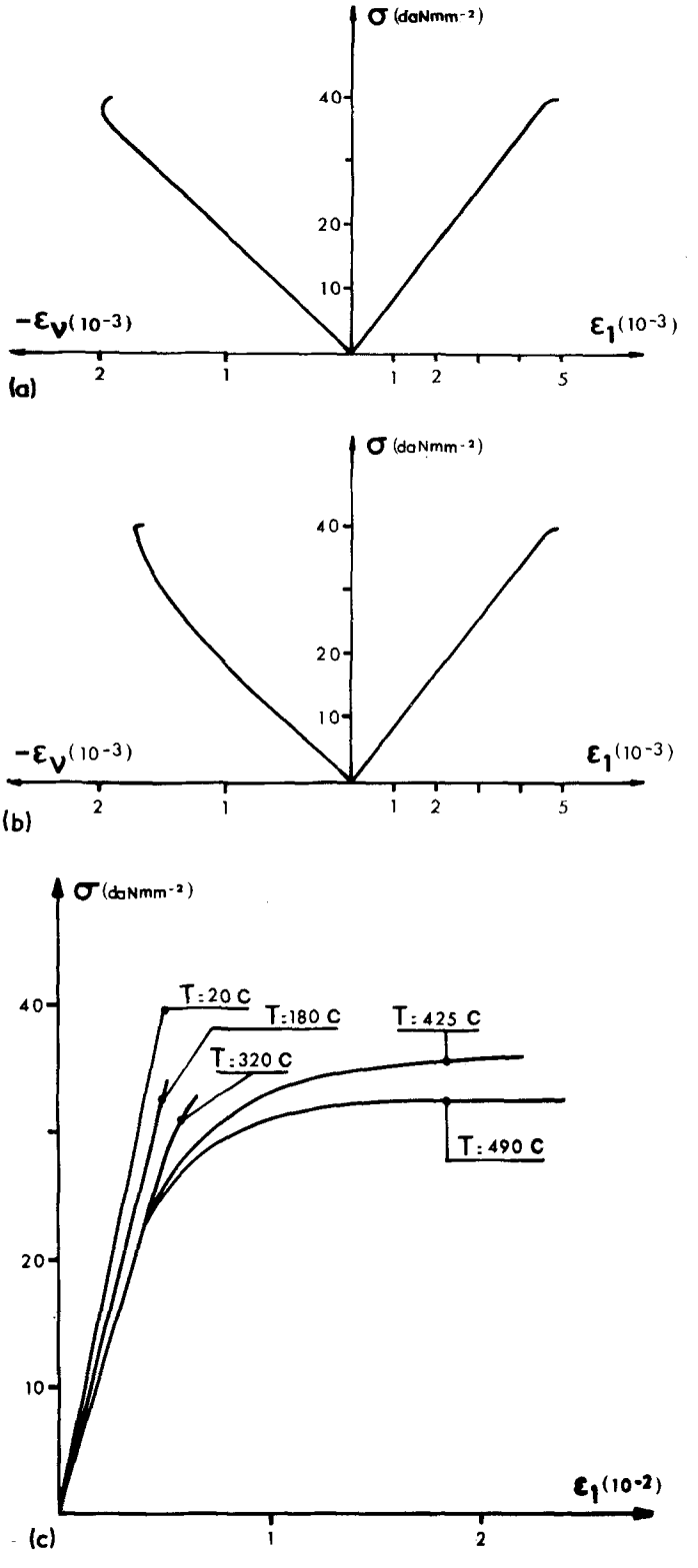

Figure 2 (a) Typical stress-strain curve at room temperature. Elastic behaviour, the slope of the curve is equal to the average Young modulus (micrite A). Corresponding stress-volumic strain curve $\sigma(\epsilon_v)$ on the left part. (b) Deviation from linear behaviour for the $\sigma(\epsilon_v)$ curve indicating a progressive opening of flaws parallel to the compression axis. (c) Typical set of stress curves $\sigma(\epsilon_1)$ for various temperatures; micrite D.

average Youngs modulus $<E> = 7000$ daN mm^{-2}*. The fracture strengths and the elastic slopes are reported in Table I. Each value is given with its dispersion for approximately 25 tests.

No trace of plasticity could be detected, even for the lowest stress rates, $\dot{\sigma} = 0.1$N mm^{-2} sec^{-1}, which can be reached with such samples using an Instron machine. The beginning of the curves did not present any fault of linearity as is often observed in rock compression experiments and is interpreted as the progressive closure of flaws, small cracks, etc [4]. A typical $\sigma(\epsilon_1)$ curve is shown in Fig. 2a with its corresponding $\sigma(\epsilon_V)$ curve. The Poisson coefficient is constant all along the curve and is equal to $\nu = 0.30 \pm 0.02$.

In some rare cases, we observed a slight deviation from the elastic linear behaviour on the $\sigma(\epsilon_V)$ curve, but this occured for high stresses (Fig. 2b) and the $\sigma(\epsilon_1)$ curve as well as the fracture strength were not significantly affected. Such samples contained probably larger initial cracks and the fact that σ_F did not decrease clearly means that fracture is governed by its propagation stage rather than by its initiation stage in our compression experiments.

2.2.2. Compression at higher temperatures

For temperatures above 300° C, a sligh plasticity is detected for high stresses and the fracture strength drops to $\sigma_F \simeq 30$daN mm^{-2} (see Table 1). The total plastic deformation reaches $\epsilon_1^P \simeq 4\%$ and $T = 500°$ C. For higher temperatures, experiments become meaningless without confining pressure, because of the rapid decomposition of the rock ($CaCO_3 \rightarrow CO_2 + CaO$). This phenomenon is perhaps responsible for the observed decrease of σ_F at temperatures below 500° C. Indeed, microscopic investigations reveal a preferential stress–induced decomposition, especially along the grain boundaries, which should favour crack propagation. Fig. 2c shows a typical set of $\sigma(\epsilon_1)$ curves for various temperatures.

The problem arises as to how to share the total plastic deformation between, on the one hand, the true plasticity involving dislocation motion (and twinning), and on the other, the deformation due to the stable and slow crack propagation governed by the chemical decomposition at the front of the crack. This is a very complicated problem which could not be solved satisfactorily. However, the number of macrocracks which developed is found to be much larger for experiments at high temperature. This shows that crack propagation is often stabilized or arrested by plastic relaxation on its front while at room temperature, only one macrocrack develops suddenly along the compression axis.

3. Microscopic observations

We have observed fresh fracture surfaces by means of carbon replicas and directly by scanning electron microscopy (SEM). It was thus possible to find at least semi-quantitatively the grain-size distribution and the fracture type (inter- or intragranular type). From many observations, we deduce the following points.

3.1. Fracture type

Fracture is always of an intergranular type when it propagates in regions with grains smaller than 3 to 4 μm. Fracture becomes intraganular when it meets larger grains and beautiful cleavages appear in such cases (Fig. 3). This difference is due to the fact that the stress including a cleavage in a grain increases when the grain size, D, decreases, $\sigma_C = K D^{-1/2}$ [5]. Both types correspond to a brittle fracture mechanism and we did not observe traces of plasticity for room temperature fractures: no river patterns on the cleaved faces which would indicate a relatively high dislocation density in the cleaved grains, no slip lines on the faces of the grains, no trace of twinning.

At higher temperatures, the intergranular type seems to be more pronounced, but the prominent fact is the "decoration" of the grain boundaries by small bubbles (Fig. 3c) caused by chemical decomposition. It is therefore impossible to detect the possible traces of plastic deformation. Moreover, there is no significative growth in grain size (the high temperature experiments lasted about 4 h).

3.2. Precipitates

The chemical analyses indicate that our micrites contain at least 95% $CaCO_3$. The main impurities found are coherent with a second phase of clay minerals, alumino silicates (for instance for micrite A, the following composition is found: $CaCO_3$ 95.9%; SiO_2 1.5%; MgO 0.7%; Al_2O_3 0.63%; Na_2O 0.05%; K_2O 0.11%; TiO_2 0.03%;

*The problem of averaging an elastic constant in a polycrystalline material can be complicated [3] but the precise value of $< E >$ is not relevant here.

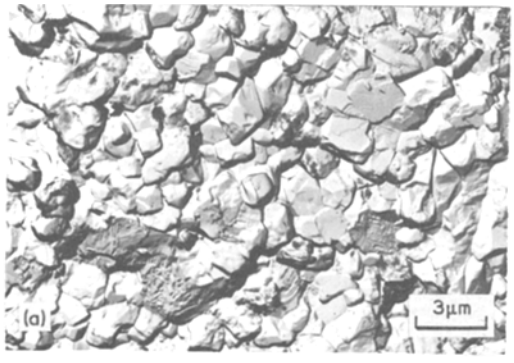

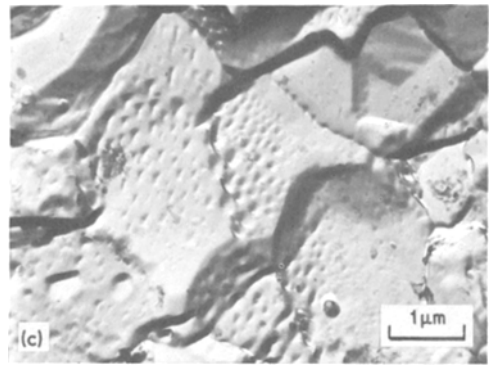

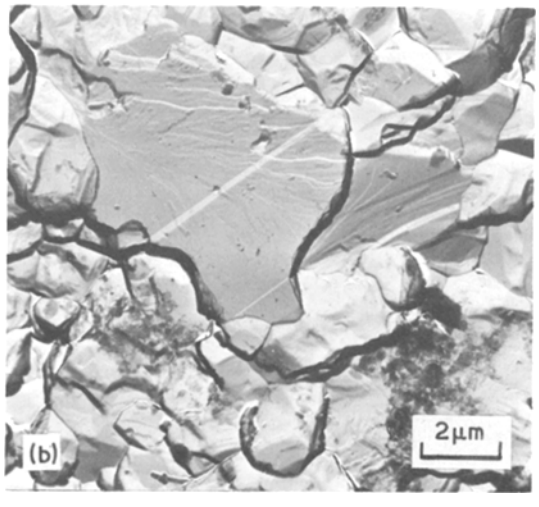

Figure 3 (a) Intergranular fracture at room temperature, region of small grains (size $\leqslant$ 3 to 4 μm). (b) Cleavage of large grains at room temperature. (c) Fracture at $T = 500^{\circ}$ C; the grain boundaries are decorated by small bubbles due to chemical decomposition.

total Fe, i.e. FeO and Fe_2O_3, 0.28%). The X-ray microprobe attachment of the SEM allowed one to visualize the impurities which are found to be concentrated in small precipitates stuck in the grain boundaries. We were able to extract these with carbon replicas and to confirm their crystalline structures (Fig. 4).

3.3. Pores

Many pores are detected by SEM on fractured faces. These pores seem to be closed and the largest ones are approximately spherical with a diameter in the order of 20 μm (Fig. 5). Fracture, when propagating, probably tends to intersect a large number of such large holes because they act as stress concentrators. Therefore, the distribution of pore diameters observed by SEM does not coincide with the one evaluated with the Hg

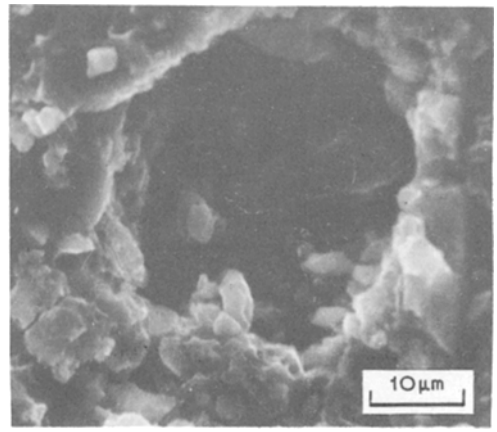

Figure 5 Closed pores detected on an SEM topograph; fractured face at room temperature.

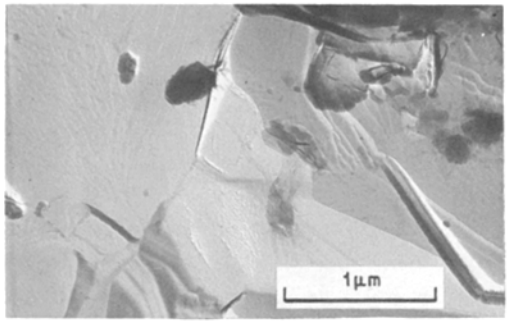

Figure 4 Clay mineral lamella extracted by carbon replica and its diffraction pattern.

porosimeter. The very abundant small pores of 100 Å, in particular, could not be detected by SEM.

3.4. Grain size

The grain sizes and the grain shapes are easily characterized by carbon replicas. One finds that for all the observed micrites, 90% of the fractured surfaces correspond to grains of 1 to 4 μm. Larger grains cover only 2% of the surface. They are systematically cleaved and their size is about 10 μm. The remaining 8% are occupied by very fine grains of 1 μm or less (Fig. 6). These are very often concentrated in clusters. The true grain-size distribution in the bulk could be different from the superficial one, because fracture surfaces are not randomly distributed in the crystal. However, the 3 μm grains are the most abundant.

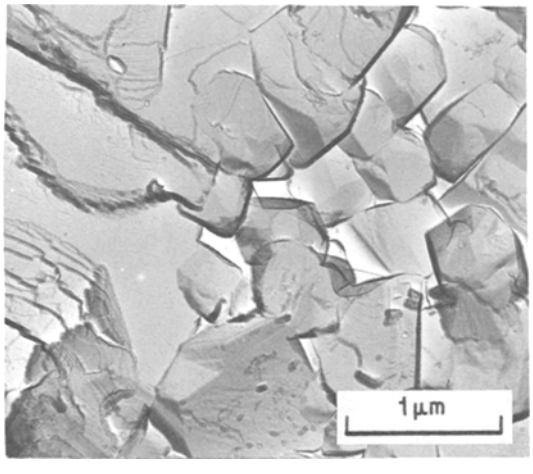

Figure 6 Cluster of very fine grains less than 1 μm.

3.5. Grain boudararies

The shape of the 3 μm grains is almost always rhomboedral. We have verified by stereography that the angles between the faces of these grains are equal to those between the $\{1\,0\,\bar{1}\,1\}$ rhomboedral faces of the calcitic cell (Fig. 7). Moreover, it is noticeable that these grains are also associated in such a way that their lattices coincide, i.e. they build coincidence boundaries of the first order [6]. There are perhaps other stable coincidence boundaries of higher orders but it is difficult to find them in this non-cubic structure. The occurrence of many coincidence boundaries between grains can play an important role in the compactness of the material.

Some other grain boundaries are not flat. In this case, steps on the faces of the grains are often observed (Fig. 8). We suggest that they have grown on initially flat rhombohedral faces in order to close the residual space lying between the non-parallel faces of two neighbouring grains. These grains were, of course, unable to rotate freely because they were probably already bonded to other grains. The pressure solution mechanism [7] and the recrystallization processes [8] can explain how they grew and thus slowly obliterated the rock.

4. Discussion

We first discuss the possible role of the observed coincidence boundaries, steps, etc, on the resulting compactness of micrites; the fracture mechanisms are then discussed.

4.1. High compactness

The end result of the lithification of micrites is a highly compact material comparable to sintered ceramics, although micrites have never been heated. This paradoxical result can be understood, however, with the following argument.

4.1.1. Precipitation

Sea water, saturated in $CaCO_3$, contains numerous solid particles of calcite. The size of the particles is limited to a relatively narrow range because the largest ones fall rapidly to the sea bottom while, for the smallest ones, there is a critical size for which they are no longer stable and re-dissolve (when the surface energy becomes larger than the free energy gained by the crystal formation). The probability for clustering of particles of similar sizes can become high when their concentration increases (because of the evaporation of the sea water for example). Moreover, owing to their Brownian motion, the particles can often associate but they cluster permanently only when they build stable grain boundaries such as coincidence boundaries. When the clusters are large enough, they sink and form the ooze. An alternative mechanism for ooze formation is the growing of individual particles, but the former mechanism is probably more rapid and only a few large grains are found in the actual micrites.

4.1.2. Lithification

The next step is the decrease of the porosity of the micrite ooze. Two mechanisms can act in addition to the vertical lithostatic pressure.

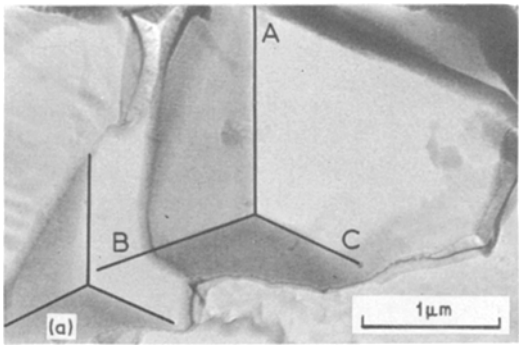

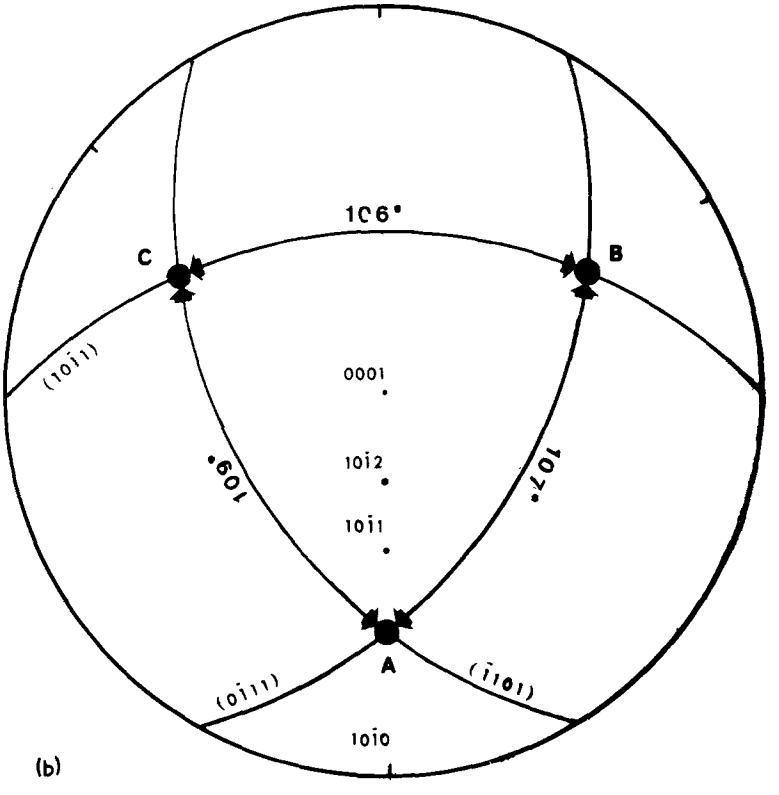

Figure 7 (a) Rhomboedral 3 μm grains associated in a coincidence boundary. (b) Stereographic projection indicating the angular relations between the external faces.

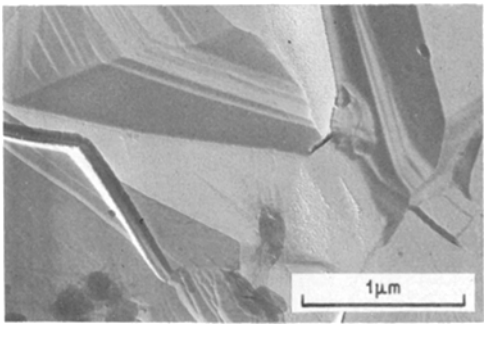

Figure 8 Steps on the opposite faces of two adjacent grains; carbon replica.

(a) Sea water, containing solid particles, flows through the ooze and is filtered by it, the largest particles being the first to be filtered. The smallest particles which have been observed on replicas (0.15 μm size) can correspond to the minimal size as far as their energetic stability is concerned. Clay particles can also be introduced into the sediment at this level.

(b) The pressure solution and the recrystallization processes occur, supplying or releasing calcite which is re-used to grow steps on the grains of adjacent clusters.

It is to be remarked that if a free space is isolated from the main fluid phase, it will never close. This explains why the rock is never fully dense.

Mechanism b presents some analogies with the mechanisms of sintering, but in the case of micrite formation, the transfer of matter is achieved at room temperature by means of a fluid phase from the surface of one grain to the surface of another. The grain boundaries do not move, there is no increase in grain size.

4.2. Fracture

We discuss successively the elastic (or plastic) part of the $\sigma(\epsilon)$ curves then their limiting value, σ_F.

4.2.1. Elastic or plastic behaviour before rupture

No trace of plastic deformation was defected for the room temperature experiments. This is not surprising because the elastic limit of calcite is large at room temperature. For the easiest glide system of single crystals, it reaches $\sigma_E = 12$daN mm^{-2} [9], and for polycrystals it can be larger than the maximum shear stress $\frac{1}{2}\ \sigma_F = 20$daN mm^{-2}. Furthermore, owing to their slow formation, micrite grains are probably almost free of dislocations (Barber and Wenk [10] verified by TEM that some Solnhofen limestones present many dislocation-free grains). A yield phenomenon is, therefore, expected with an upper elastic limit which could be larger than $\frac{1}{2}\ \sigma_F$.

At higher temperatures, the elastic limit decreases; it falls to $\sigma_E = 2$daN mm^{-2} at 500° C for single crystals [9] and the dislocation motion in our polycrystalline samples is only limited by the compatibility problems at the grain boundaries.

4.2.2. Fracture strength at room temperature

There are many pre-existing defects which can initiate a crack (closed pores, clay mineral precipitates, steps, especially in the vicinity of a closed pore, etc). The micrographs indicate that the fracture surface intersects many such defects, but the conventional Griffith criterion, $\sigma_F = K\sqrt{(E\gamma/\epsilon)}$, which has been developped for tensile sollicitations [11], cannot be used here and all the defects are relevant. Indeed, in the energy balance equation postulated by Griffith, the elastic energy to be relaxed by the crack propagation depends upon the stress distribution around the defect, and this distribution is very different in the tensile and in the compressive cases. In the former case, the high tensile region extends all around the defect in a plane perpendicular to the tensile axis. On the other hand, in the compressive case, this region is much smaller (it is confined to two small domains at the intersections of the compression axis with the defect [12]. A very high fracture strength should thus result, but we have to take into account the distribution of defects which produce some overlapping of the tensile regions in such a way that an unstable propagation becomes possible when the applied stress reaches the value σ_F. This value is a complicated function of the defect distribution in size, in shape and in mean distance which cannot be calculated quantitatively. The small dispersion observed in Table I for the σ_F values at room temperature, is probably due to the fact that we are concerned with some king of averaging over all the defects along the path of the fracture surface.

If a slight stable crack propagation occurs before fracture, the slopes of the $\sigma(\epsilon)$ curve have to decrease. The dispersion of the elastic slopes reaches 10% for all tests on the four micrites while imprecisions of the measurements are less than 2%. However, two other phenomena can modify the slopes $d\sigma/d\epsilon$.

(a) Holes produce a decrease of the elastic compliances. This variation depends on the size distribution of the holes. If we assume that the open porosity spectrum in Fig. 1 can be extended to the total porosity, micrite C, which exhibits the largest spectrum, should suffer the largest decrease of $d\sigma/d\epsilon$ as effectively observed (Table 1).

(b) A non-isotropic texture of our polycrystalline materials changes the mean value $<E>$. We have detected a slight anisotropy in compressing samples cut along different directions relative to the stratigraphic plane. An anisotropy index, defined as the maximum relative variation of the slope $d\sigma/d\epsilon_1$, is reported in Table 1. Its magnitude is of the order of the observed dispersion.

Therefore, the possible stable crack propagation before fracture cannot be detected except in some rare cases on the $\sigma(\epsilon_V)$ curves, as for example on Fig. 2b.

Acknowledgements

The authors thank the CNRS for their financial support. They also thank Dr J.P. Poirier and Dr G. Martin of C.E.N. Saclay for the fruitful

discussions they have had with them, and Dr P. Debrabant who performed the chemical analyses.

References

1. R. G. C. BATHURST, "Carbonate sediments and their diagenesis" (Elsevier, Amsterdam, (1971) p. 321
2. For the geological setting of the studied micrites, see the geological maps:
   Micrites A and B: ORNANS (1/50.000) edited by B.R.G.M. (1966)
   Micrite C: FIGEAC (1/80.000) no. 195, edited by B.R.G.M.
   Micrite D: Bull. B.R.G.M., section II no. 1 (1970) by P. BERNER *et al.*
3. J. P. HIRTH and J. LOTHE "Theory of crystal dislocations" (McGraw Hill, New York, (1968) p. 399.
4. J. C. JAEGER and N. G. W. COOK "Fundamentals of rock mechanics" (Methuen, London, 1969) p. 74.
5. A. S. TETELMAN and A. J. McEVELY "Fracture of structural materials" (Wiley, New York, 1967) p. 194.
6. W. BOLLMANN, "Crystal defects and crystalline interfaces" (Springer Verlag, Berlin, 1970) p. 413.
7. M. A. PATERSON. *Rev. Geophys. Space Phys.* **11** (1973) 355.
8. D. WACHS and J. HEIN, *J. Sed. Petrology* **44** (1974) 1217.
9. J. MUNIER, Thesis, Université de Lyon (1973).
10. D. J. BARBER and H. R. WENK, *J. Mater. Sci.* 8 (1973) 500.
11. P. C. PARIS and G. C. SIH in "Fracture thoughness testing", A.S.T.M. S.T.P. 381 (1966) p. 30.
12. A. I. LUR'E, "Three dimensional problems in the theory of elasticity" (Interscience, New York, 1964) p. 350.

Received 8 December 1975 and accepted 17 March 1976.